Article

Discovery Medicine 2025; 37(193): 383–393
https://doi.org/10.24976/Discov.Med.202537193.31

Development of a Radiomic Model to Detect the Retromolar Canal on Panoramic Radiographs

Dongjing Zhan[1,2,3], Fei Wang[4], Donglin Zeng[1,2,3], Lili Hao[1,2,3], Li Ye[1,2,3], Yipin Qi[1,2,3,*], Qiong Xu[1,2,3,*]

[1]Hospital of Stomatology, Sun Yat-sen University, 510055 Guangzhou, Guangdong, China
[2]Guangdong Provincial Key Laboratory of Stomatology, 510055 Guangzhou, Guangdong, China
[3]Guanghua School of Stomatology, Sun Yat-sen University, 510055 Guangzhou, Guangdong, China
[4]Department of Oral and Maxillofacial Surgery, Nanfang Hospital, Southern Medical University, 510515 Guangzhou, Guangdong, China
*Correspondence: qiyp3@mail.sysu.edu.cn (Yipin Qi); xqiong@mail.sysu.edu.cn (Qiong Xu)
Published: 20 February 2025

Background: The retromolar canal (RMC) is an extension of the mandibular canal located in the distal region of the mandibular third molar. Accurately detecting the RMC using conventional two-dimensional images is challenging, potentially leading to anesthetic failure and sensory disorders. This study aims to explore the clinical application of a radiomic model based on panoramic radiographs in detecting the RMC.

Methods: A retrospective collection of cone beam computed tomography (CBCT) and panoramic radiographs was conducted on 800 patients, covering 1555 hemimandibles. CBCT images served as the gold standard for confirming the presence of RMC. A dataset comprising 846 retromolar regions was established for model training and testing, with an 8:2 ratio. On the panoramic radiographs, the retromolar regions were delineated as the regions of interest, and radiomic features were extracted and selected. Support vector machine (SVM), logistic regression (LR), k-nearest neighbors (KNN), and multilayer perceptron (MLP) were employed to construct detection models for the RMC. The performance of these algorithms was assessed using receiver operating characteristic (ROC) curves, calibration curves, and decision curve analysis (DCA), and the area under the receiver operating characteristics curve (AUC) values were compared with those of a dentist and a radiologist.

Results: The RMC was identified in 423 (27.2%) out of 1555 hemimandibles on CBCT images. The four algorithms, particularly SVM and MLP, demonstrated outstanding classification abilities in detecting the RMC, with AUC values ranging from 0.831 to 0.895 in the training set and from 0.719 to 0.808 in the testing set. These results significantly surpassed those of the dentist and radiologist ($p < 0.05$).

Conclusion: Radiomics based on panoramic radiographs exhibit a high detection capability for the RMC, emphasizing its considerable clinical application value.

Keywords: retromolar canal; radiomics; cone beam computed tomography; panoramic radiographs; detection

Introduction

The retromolar canal (RMC) is a branching structure that originates from the mandibular canal at the distal region of the mandibular third molar. After diverging from the main trunk of the mandibular canal, it ascends posteriorly and opens in the retromolar region, forming the retromolar foramen (RMF) [1]. The discovery of the RMC dates back to 1967 when it was first observed during cadaver dissection [2]. It is considered a structural variant resulting from incomplete fusion of the fetal mandibular canal [3]. The RMC contains vascular nerve bundles primarily composed of myelinated nerves originating from the mandibular canal, along with fine arterioles and veins [2,4]. The intricate structure of the RMC increases the risk of complications during oral procedures in the retromolar region, such as mandibular third molar extraction, fracture reduction, and orthognathic surgery. Complications related to the RMC include failure of local anesthesia, unexpected bleeding during surgery, and postoperative sensory disorders of the buccal gingiva in the molar area [5–7]. Hence, preoperative detection of the RMC is crucial for minimizing these complications.

As a concealed bony anatomical channel within the mandible, the RMC is not easily identifiable through general radiographic examination. Currently, cone beam computed tomography (CBCT) stands as the most effective method for detecting the RMC, offering clear three-dimensional images of oral hard tissues and precise visualization of the anatomical structure of the mandibular canal and its branches. However, the clinical application of CBCT is limited by its high radiation dose, elevated cost, and complex operation, rendering it unsuitable as a routine screening method for RMC. Panoramic radiographs are

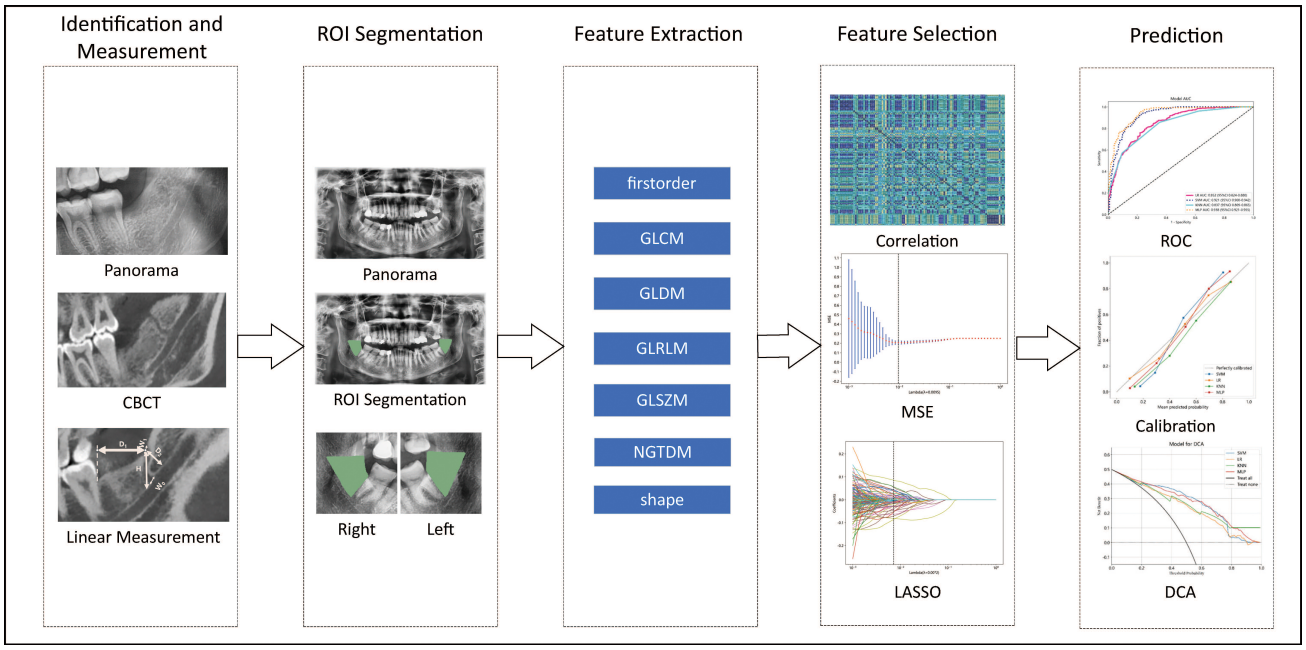

Fig. 1. The workflow of radiomic analysis in this study involved several key steps. Firstly, the recognition and measurements of the retromolar canal (RMC) on cone beam computed tomography (CBCT) were conducted, and the regions of interest were delineated on the panoramic films. Subsequently, various radiomic features were extracted from these regions of interest, encompassing first-order features, shape features, gray-level co-occurrence matrix (GLCM) features, gray-level dependence matrix (GLDM) features, gray-level run length matrix (GLRLM) features, gray-level size zone matrix (GLSZM) features, and neighborhood gray-tone difference matrix (NGTDM) features. Following feature extraction, intergroup correlation coefficients, Spearman correlation coefficients, and the least absolute shrinkage and selection operator (LASSO) methods were employed to select the most relevant features. Finally, the model was evaluated using the receiver operating characteristic (ROC) curve, calibration curve, and decision curve analysis (DCA) curve. MSE, mean squared error.

widely utilized in oral clinical examinations due to their ability to capture a broad array of anatomical structures, encompassing the full dental arch, jawbone, nasal cavity, maxillary sinus, and temporomandibular joint, all in a single exposure. Nevertheless, the two-dimensional images in panoramic radiographs are often subject to geometric distortion and interference from overlapping tissues. While several studies have attempted to visualize the RMC using panoramic radiographs, the accuracy remains limited, with over 70% of the structures remaining unidentified [8–10]. Hence, there is a pressing need for an efficient and cost-effective image analysis method to enhance the diagnostic capabilities of panoramic radiography for detecting the RMC.

Radiomics entails the conversion of digital medical images into analyzable data by extracting quantitative image features based on shape, intensity, and texture [11]. The amalgamation of radiomics and dentistry has demonstrated significant potential in oral diagnosis and treatment in recent years. Oral imaging data, including panoramic films, periapical films, bitewing films, and CBCT, have been utilized to construct radiomic models in various fields such as endodontics [12], maxillofacial tumors [13], orthodontics [14], oral implantation [15], prosthodontics [16], and temporomandibular joint disease [17]. These models exhibit enhanced precision and efficiency in judgment capabilities compared to traditional manual film interpretation. However, no radiomic model based on panoramic imaging has been developed for the detection of RMC.

In the present study, we initially evaluated the incidence, type, and anatomical characteristics of the RMC through the analysis of CBCT images. Subsequently, we developed a radiomic detection model based on panoramic radiographs to assess the presence of the RMC, utilizing CBCT identification as the gold standard.

Materials and Methods

Patients and Study Design

The research data consisted of CBCT and panoramic radiographs from 800 patients (1555 sides, 780 left and 775 right) who visited the Hospital of Stomatology, Sun Yat-sen University between January 2022 and April 2023. Inclusion criteria were as follows: (1) Age $\geq$18 years; (2) Symmetrical maxillofacial region with no deformities or severe traumatic or surgical history affecting the shape of the mandibles; (3) Clear CBCT images with a complete field of view and no significant metal artifacts. Exclusion criteria

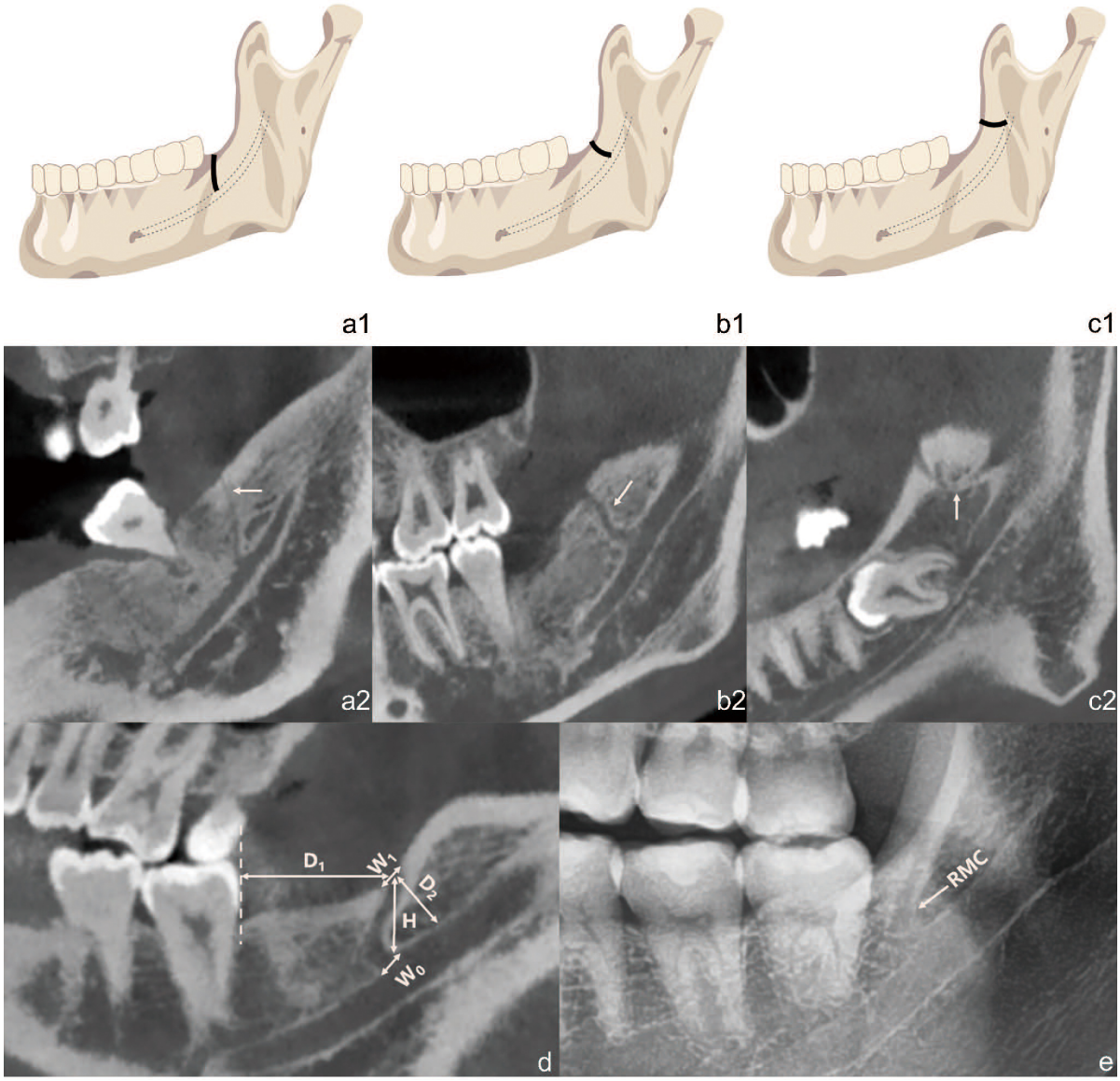

Fig. 2. Classification of RMC according to the course (arrow). Type A (a1,a2), a vertical course. Type B (b1,b2), is a curved course. Type C (c1,c2), a horizontal course (including the RMCs branched from the independent mandibular foramen). Linear measurement on sagittal CBCT images (d). Distance from retromolar foramen (RMF) to mandibular second molar (D_1); Distance from RMF to mandibular canal (D_2); Height of RMC (H); Starting width of RMC (W_0); Width of RMF (W_1). Trace of RMC (arrow) on panorama (e) of the same patient.

included: (1) Patients with mandibular trauma or surgery severely affecting the shape of the mandibles; (2) Patients with obvious space-occupying lesions such as mandibular cysts or tumors; (3) CBCT images with significant metal artifacts; (4) Patients with severe periodontitis or osteomyelitis of the jaw; (5) Mandibular sides missing second and third molars. The study design and pipeline are depicted in Fig. 1.

CBCT and Panorama Scanning Techniques

The CBCT images of patients were assessed using a CBCT scanner (NewTom VGI, QR srl Inc., Verona, Italy) in the radiology department of the Hospital of Stomatology, Sun Yat-sen University. The CBCT scanning parameters were as follows: Spatial resolutions: 0.300 mm, tube voltage: 110 kV, tube current: 3.00 mA, field of view: 15 cm $\times$ 12 cm, exposure time: 1.8 s. Panoramic radiographs were captured using computed tomography (PHT-6500, Vatech, Hwaseong, Korea) with standard parameters of tube voltage at 90 kV and tube current at 10 mA. During CBCT and panoramic imaging, each patient was positioned upright with their head stabilized using head supports. The Frankfurt plane was oriented parallel to the floor plane, and the facial midline was perpendicular to the ground plane.

Confirmation of the RMC

Two trained dentists (Q.X. and F.W., with over 20 and 8 years of clinical experience, respectively) conducted simultaneous evaluations of the retromolar area on CBCT. The observed area extended from one side of the mandibular foramen to the distal region of the mandibular third or second molar on the same side. If a branch of the mandibular canal was found to open to the RMF in this region, it was recorded as the presence of RMC. In cases of disagreement, a radiologist (Donglin Z, with over 20 years of experience) made the final decision. To construct the detection model, a dataset was comprised of 423 mandibular sides diagnosed with the presence of RMC, combined with an equal number of samples without RMC randomly selected from the 1132 mandibular sides on CBCT images. The dataset, consisting of 846 mandibular sides, was then randomly divided into training (337 sides with RMC and 339 sides without RMC) and testing sets (86 sides with RMC and 84 sides without RMC) at an 8:2 ratio.

Classification and Linear Measurements of the RMCs

The RMCs identified in 423 mandibular sides were classified into three categories based on their course and morphology according to VON's classification [1]: Type A (vertical course), Type B (curved course), and Type C (horizontal course) (Fig. 2a1–c2). From sagittal CBCT images, the following measurements were obtained: (1) Distance from RMF to mandibular second molar (D_1): the horizontal distance from the midpoint of the RMF to the distal edge of the enamel-dentin junction of the mandibular second molar; (2) Distance from RMF to mandibular canal (D_2): the shortest distance from the RMF to the mandibular canal; (3) Height of RMC (H): the vertical distance from the midpoint of the RMF to the upper border of the mandibular canal; (4) Starting width of RMC (W_0): the width of the starting point of the RMC; (5) Width of RMF (W_1); (6) The average value of W_0 and W_1 was defined as the width of the RMC (Fig. 2d). These measurements and classifications were performed by a trained dentist (F.W., with over 8 years of clinical experience). Fig. 2e displays the potential trace on the panorama, which is likely the trace of RMC.

Region of Interest Segmentation and Image Preprocessing

The panoramic images of 846 mandibular sides were initially resampled to a voxel resolution of $1 \times 1 \times 1$ mm^3. A dentist (L.H., with over 8 years of clinical experience) manually outlined the retromolar area on the panoramic images using ITK-SNAP (version 3.6.0, http://www.itksnap.org/pmwiki/pmwiki.php) in a blinded fashion. The boundaries of the retromolar area were defined as follows: the distal boundary was the mandibular foramen, the mesial boundary was the distal aspect of the mandibular second or third molar, the lower boundary was the upper border of the mandibular canal, and the upper boundary was the upper edge of the mandible (Fig. 3a,b). To verify the reproducibility of the outlining process, 30 mandibular sides were randomly selected, and a dentist (Y.Q., with over 15 years of clinical experience) independently re-outlined the retromolar area. These steps were taken to ensure a reliable and representative dataset for the subsequent analysis and development of the radiomics model.

Radiomic Feature Extraction and Selection

Radiomic features were extracted from regions of interest using Python software (version 3.7.12; Python Software Foundation, Wilmington, DE, USA). The handcrafted features were categorized into three primary groups: (I) geometry, (II) intensity, and (III) texture. The geometry features capture the shape characteristics of the region, while the intensity features describe the first-order statistical distribution of voxel intensities within the region. The texture features delineate the patterns or spatial distributions of intensities, encompassing second and higher-order information. There are five categories of texture features, including the gray-level co-occurrence matrix (GLCM), gray-level dependence matrix (GLDM), neighborhood gray-tone difference matrix (NGTDM), gray-level size zone matrix (GLSZM), and gray-level run length matrix (GLRLM).

To ensure comparability, all extracted features were normalized to a range between 0 and 1. Next, a four-step procedure was carried out to select relevant radiomics features and reduce dimensionality in the training set. Firstly, invalid features, including null values, infinite values, and those with zero variance, were eliminated. Secondly, the intraclass correlation coefficient (ICC) was calculated for each radiomic feature to assess reproducibility. Features with an ICC value greater than 0.75 were considered reproducible and robust. Thirdly, Spearman's rank correlation coefficient was utilized to measure the correlation between features. If the correlation coefficient between any two features exceeded 0.9, only one of the correlated features was retained. Finally, the least absolute shrinkage and selection operator (LASSO) regression model, a regularization method that effectively selects features and reduces overfitting, was employed to construct a signature using the remaining features from the previous steps.

Radiomic Model Development and Evaluation

After feature screening, the final retained features were utilized to build machine learning algorithms, including logistic regression (LR), support vector machine (SVM), k-nearest neighbors (KNN), and multilayer perceptron (MLP). The classification ability of the radiomic model was evaluated using the area under the receiver operating characteristics curve (AUC) values and their corresponding 95% confidence intervals (CI). Calibration curves were plotted to compare the predicted and actual values. Decision curve analysis (DCA) curves were conducted to demonstrate the clinical usefulness of the detec-

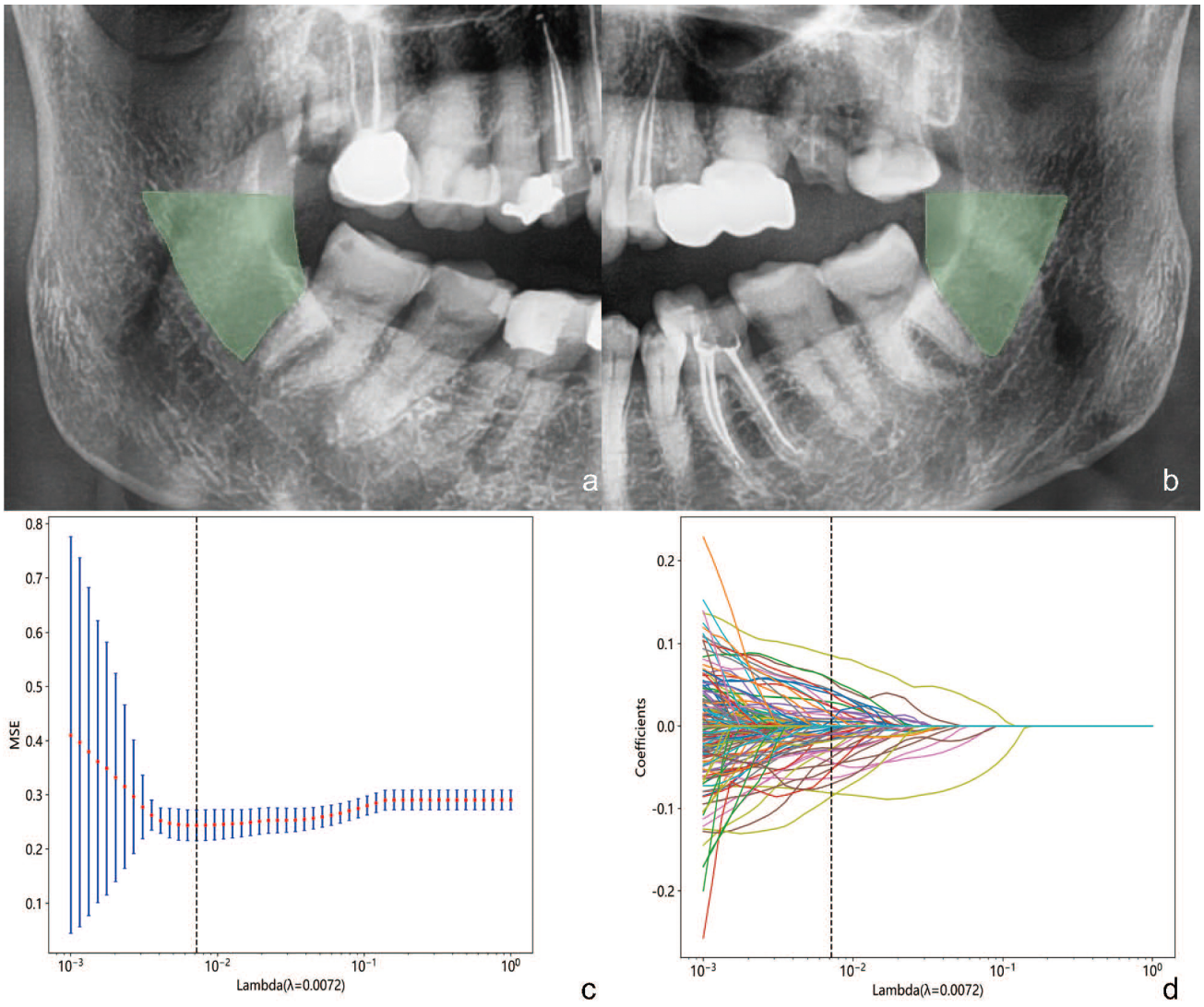

Fig. 3. Region of interest delineation and LASSO-based radiomic feature selection. The region of interest in the left (a) and right (b) sides: the distal boundary was the mandibular foramen, the mesial boundary was the distal of the last mandibular molar, the lower boundary was the upper border of the mandibular canal, and the upper boundary was the upper edge of the mandible. Radiomic feature selection based on the LASSO model: ten-fold cross-validated coefficients (c) and ten-fold cross-validated mean squared error (MSE) (d).

tion model. The accuracy, sensitivity, specificity, F1 score, positive predictive value (PPV), and negative predictive value (NPV) of these algorithms were calculated.

Comparative Analysis of Diagnostic Performance between the Radiomic Model and Specialists

To compare the detection performance of the radiomic model with the diagnosis made by human observers, a dentist (Dongjing Z, with 4 years of clinical experience) and a radiologist (Donglin Z, with over 20 years of experience) independently evaluated the panoramic images in the testing set. The accuracy, sensitivity, specificity, F1 score, PPV, NPV, and AUC of the observers were calculated. The DeLong test was employed to compare the AUC values between the radiomic model and human observers.

Statistical Analyses

Statistical analyses were conducted using Python software (version 3.7.12; Python Software Foundation, Wilmington, DE, USA) and SPSS (version 25.0; IBM Corporation, Armonk, NY, USA). To assess the consistency of judgments between the two dentists regarding the RMC, the kappa value was calculated. Pearson Chi-square tests were performed to analyze the statistical differences among gender, age, and lateral distribution of the RMC. The Shapiro-Wilk test and Levene's test were used to assess normal distribution and homogeneity of variance. For variables that did not conform to a normal distribution, including the starting width of RMC, width of RMF, and width of RMC, the results were presented using the median (interquartile range [IQR]). For variables that followed a normal distri-

Table 1. Gender, age, and lateral distribution of the RMCs.

	Presence	Absence	Total	Incidence	χ^2 value	*p*-value
Gender (n = 800)						
Male	151	258	409	36.92%		
Female	146	245	391	37.34%	0.02	0.90
Age/Year (n = 800)						
18–40	152	305	457	33.26%		
41–60	111	151	262	42.37%		
>61	34	47	81	41.98%	6.82	0.03
Lateral (n = 1555)						
Left	213	567	780	27.31%		
Right	210	565	775	27.10%	0.01	0.93

Table 2. Linear measurement data of the RMCs and RMFs (mm).

	Mean ± SD	Median [IQR]
Starting width of RMC	-	1.50 [0.80]
Width of RMF	-	0.70 [0.50]
Width of RMC	-	1.10 [0.55]
Height of RMC	16.24 ± 3.34	16.20 [4.30]
Distance from RMF to the second molar	13.26 ± 3.10	13.50 [4.28]
The shortest distance from RMF to the mandibular canal	9.54 ± 2.05	9.50 [2.60]

SD, standard deviation; IQR, interquartile range.

bution, such as the height of RMC, distance from RMF to the second molar, and the shortest distance from RMF to the mandibular canal, the results were presented using both mean ± standard deviation (SD) and median [IQR] values. A *p*-value of less than 0.05 was considered statistically significant.

Results

The Prevalence and Classification of the RMCs

The patients included comprised 391 females and 409 males, with an average age of 39.5 years and an age range from 18 to 84 years. The agreement between the two dentists regarding the presence of the RMC on CBCT was substantial, as indicated by a kappa value of 0.885. Out of the 1555 sides of the mandibles observed on CBCT, 423 sides (27.2%) showed the presence of RMCs. Among these, 213 cases were on the left side, and 210 cases were on the right side. There were 126 individuals who had RMCs on both sides, 171 individuals with RMCs on only one side, and a total of 297 individuals (37.1%) with at least one side exhibiting RMCs. In terms of morphological classification, 165 sides (39.01%) were classified as Type A (vertical), 242 sides (57.21%) as Type B (oblique), and 16 sides (3.78%) as Type C (horizontal).

The prevalence of RMCs was 36.92% in males and 37.34% in females, with no significant difference observed ($p = 0.90$). When considering age groups, the prevalence of RMCs in the youth group (18–40 years old), middle-aged group (41–60 years old), and elderly group (over 61 years old) was 33.26%, 42.37%, and 41.98%, respectively. Significant differences were noted between the three age groups ($p = 0.03$). Moreover, RMCs were observed in 27.31% of the left sides and 27.10% of the right sides, with no significant difference between the two sides ($p = 0.93$) (Table 1).

Linear Measurement Data of the RMCs

The linear measurements of RMCs on CBCT images are summarized in Table 2. The median starting width of the RMC, width of RMF, and width of RMC were 1.50 mm, 0.70 mm, and 1.10 mm, respectively. The mean height of the RMC was 16.24 mm, with a median height of 16.20 mm. The mean distance from RMF to the second molar was 13.26 mm, and the median distance was 13.50 mm. The mean shortest distance from RMF to the mandibular canal was 9.54 mm, with a median value of 9.50 mm.

The Performance of Panorama-Based Radiomic Model and Specialists in Predicting the RMC

A total of 1561 handcrafted features were extracted from the panorama, including 14 geometry features, 306 intensity features, 374 GLCM features, 238 GLDM features, 272 GLRLM features, 272 GLSZM features, and 85 NGTDM features. These features underwent a four-step feature-selection procedure. In the first step, 663 invalid features were excluded. Secondly, 163 unproducible features were excluded. In the third step, 526 features were further excluded to avoid redundancy. Finally, the LASSO classifier selected 52 features from the remaining 209 features for model construction (Fig. 3c,d).

Table 3. Performance of radiomic model and specialists.

Algorithm	Group	AUC	95% CI	Accuracy	Sensitivity	Specificity	PPV	NPV	F1
SVM	train	0.895	0.8700–0.9193	0.818	0.816	0.820	0.818	0.818	0.817
SVM	test	0.794	0.7247–0.8628	0.718	0.698	0.738	0.732	0.705	0.714
LR	train	0.831	0.8003–0.8611	0.757	0.774	0.740	0.748	0.768	0.761
LR	test	0.793	0.7261–0.8594	0.700	0.744	0.655	0.688	0.714	0.715
KNN	train	0.847	0.8200–0.8741	0.765	0.858	0.673	0.722	0.826	0.784
KNN	test	0.719	0.6442–0.7935	0.665	0.733	0.595	0.649	0.685	0.689
MLP	train	0.892	0.8685–0.9156	0.808	0.831	0.785	0.793	0.824	0.812
MLP	test	0.808	0.7410–0.8741	0.741	0.756	0.726	0.739	0.744	0.747
Dentist	test	0.542	0.4666–0.6167	0.541	0.500	0.583	0.551	0.533	0.524
Radiologist	test	0.565	0.4902–0.6399	0.565	0.535	0.595	0.575	0.556	0.554

SVM, support vector machine; LR, logistic regression; KNN, k-nearest neighbors; MLP, multilayer perceptron; AUC, area under the receiver operating characteristics curve; PPV, positive predictive value; NPV, negative predictive value.

Table 3 provides an overview of the performance metrics of different algorithms in both the training and testing sets. The SVM and MLP algorithms achieved the highest AUC values of 0.895 and 0.892 in the training sets, and 0.794 and 0.808 in the testing sets (Fig. 4a,b). The LR and KNN algorithms achieved AUC values of 0.831 and 0.847 in the training sets, and 0.793 and 0.719 in the testing sets (Fig. 4b). Furthermore, in the testing set, the four algorithms demonstrated accuracy ranging from 0.665 to 0.741, sensitivity from 0.698 to 0.756, specificity from 0.595 to 0.738, PPV from 0.649 to 0.739, NPV from 0.685 to 0.744, and F1 score from 0.689 to 0.747. The SVM and MLP algorithms showed robust and balanced performance as all metrics were above 0.7, while the LR and MLP algorithms achieved high sensitivity (0.733–0.744) but low specificity (0.595–0.655). In contrast, the performance of human judgments by a dentist with 4 years of clinical experience and a radiologist with over 20 years of experience yielded lower AUC values of 0.542 and 0.565. There was no significant difference in performance between the two observers ($p = 0.65$). The AUC values of all four algorithms were significantly better than those of the two observers ($p < 0.05$). In terms of clinical benefits, DCA curves demonstrated the advantages of the four algorithms, particularly the LR, SVM, and MLP, in most testing set circumstances (Fig. 4c). The calibration curves of the four algorithms showed good agreement between the predicted probabilities and the actual rates in the testing sets (Fig. 4d).

Discussion

The detection of the RMC presents challenges due to its hidden location and varied anatomical orientation. In this study, we developed a prediction model to enhance the RMC-detecting ability of panoramic radiographs using four different machine-learning methods. Our results revealed that all four strategies, especially SVM and MLP, exhibited excellent predictive ability and surpassed the performance of experienced imaging-specialized experts.

The RMC plays a crucial role in innervating various regions, including the retromolar triangle and buccal mucosa of mandibular molars [2,4]. Failure to consider the existence of this canal may lead to complications such as incomplete anesthesia and postoperative loss of sensation. It is recommended to use Gow-Gates high-block anesthesia in patients with retromolar canals [10]. In patients with acute pulpitis of the mandibular first molar, the adjunctive use of retromolar canal infiltration anesthesia can significantly alleviate pain when only inferior alveolar nerve block anesthesia is employed [18]. There have been reports of reduced sensation in the buccal gingiva of the molar area following sagittal split ramus osteotomy and extraction of the third mandibular molar as a result of intraoperative damage of the retromolar canal [6,19,20]. Various methods have been utilized to discover the RMC, including micro-CT [21], electron microscopy [22], CBCT [23], and panoramic radiographs [6]. The first two methods are primarily conducted in cadaver mandibles while CBCT and panoramic radiographs are commonly applied in clinical diagnosis and research. The reported incidence rates of the RMC in different CBCT studies vary significantly, ranging from 8.5% to 65.4% [1,6,8,9,21,24–30].

This wide range of variation may be attributed to differences in ethnicities, CBCT spatial resolution and image quality, and the number of samples studied. Despite these discrepancies, CBCT remains the most effective tool for detecting the retromolar canal owing to its ability to provide three-dimensional anatomical information [21]. In our study, by analysis of CBCT images, the prevalence of the RMC was found to be 27.2%, and the rate in the youth group was significantly lower than that of the middle-aged group and elderly group. This finding might be attributed to insufficient marginal ossification in young individuals, making it difficult to identify the RMC. In the present study, the distance from the RMF to nearby structures was measured. The results showed that the mean horizontal distance from the RMF to the distal edge of the enamel-dentin junction of the second molar was 13.26 mm, which is consistent with research on the Eastern Asian population (11.9 mm to

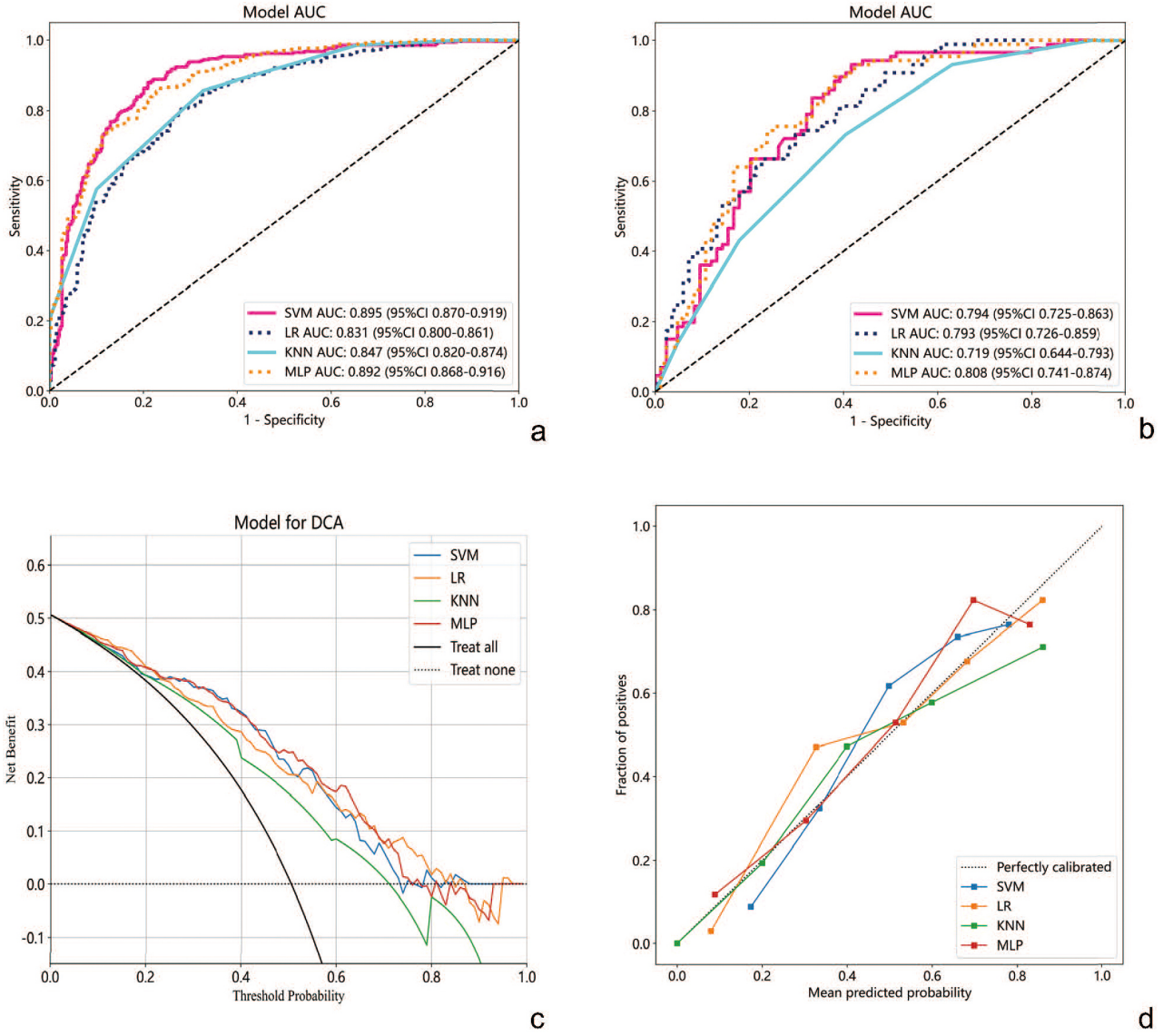

Fig. 4. Performance of radiomic model. ROC curves of the LR, SVM, MLP, and KNN algorithms in the training sets (a) and the testing sets (b); DCA curves (c) and calibration curves (d) of the LR, SVM, MLP, and KNN algorithms in the testing sets.

13.13 mm) [6,8,21] and shorter than that in European studies (15.16 mm to 15.45 mm) [1,9], indicating differences between ethnicities. The shortest distance between RMF and the mandibular canal was measured for the first time, i.e., less than 10 mm, emphasizing the need for operators to pay attention to the protection of the mandibular canal in patients with RMC during surgical procedures. These findings, derived from a large sample size of 1555 mandibular sides, provide valuable insights into the anatomical characteristics of retromolar structures.

The panoramic radiograph has been previously utilized by some researchers to identify RMCs, as it offers more convenience for clinical use and poses lower radiation risk at a lesser expense compared to CBCT scans [10]. However, the detection rate of RMCs in panoramic radiographs ranges from 0% to 5.8%, significantly lower than that of CBCT scans [1,6,9,29,31,32]. The limited detection percentage of RMCs in panoramic radiographs may be attributed to its inherent limitations, including lower resolution, imaging distortion, and interference from adjacent tissues (e.g., the mandibular lingual groove and oblique line of the mandible). In the present study, the accuracy of two observers in identifying RMCs in panoramic radiographs was found to be relatively low at 0.541 and 0.565 [10], further underscoring the challenges associated with accurate identification irrespective of experience levels. In recent years, the integration of radiomics in dentistry has significantly improved the accuracy of diagnostic judgments while reducing medical costs and time [12].

Researchers have successfully extracted radiomic features from panoramic radiographs to obtain additional disease information and develop radiomics models that outperform dentists in diagnosing various dental conditions. For example, radiomics models show superior performance in

predicting additional distal roots of the mandibular second molar [33], C-shaped root canals of the mandibular second molar [34], osteoporosis [35], dental caries [36], age group [37], and periodontal bone loss [38]. These studies employed multiple algorithms to identify the most suitable strategies for their respective objectives. In our study, we aimed to enhance the accuracy of RMC detection on panoramic radiographs and utilized well-established machine learning algorithms, including SVM, LR, KNN, and MLP. SVM is a discriminative classifier known for finding the optimal hyperplane to separate classes with a maximum margin. It is particularly effective when dealing with high-dimensional data and non-linear decision boundaries. MLP, on the other hand, is a powerful neural network model consisting of multiple layers of interconnected nodes and is capable of capturing complex relationships between input and output variables. LR is a classical linear classifier that models the probability of binary outcomes, while KNN is a non-parametric algorithm that classifies based on the majority vote of the k nearest neighbors, making it suitable for small datasets [39].

In the present study, these algorithms yielded promising results. The AUC values obtained from all four algorithms were significantly higher than those achieved by two human observers, showcasing the superiority of the radiomic model over human visual assessment in detecting the RMC [10]. MLP and SVM exhibited the highest AUC values in both the training set and testing set. This demonstrates their proficiency in handling intricate radiomic features, suggesting their suitability for this task. The LR and KNN algorithms showed relatively low specificity, indicating a higher tendency for misdiagnosing RMC. It is important for users to exercise caution in interpreting results and consider the potential of false positives when using these algorithms. The exploitation of our radiomic detection model may be beneficial in identifying patients who may require specific methods of local anesthesia or advanced imaging techniques, such as CBCT scans [10]. The American Dental Association emphasizes the judicious use of CBCT scans based on thorough patient history collection and initial two-dimensional imaging data, discouraging its routine use as a screening tool [40]. By employing the radiomic model to improve the diagnostic capabilities of panoramic radiographs, clinicians can make more informed decisions regarding the need for additional imaging, aligning with the principles of precision medicine.

Despite the enhanced detection rate of RMCs on panoramic radiographs in our research, this manuscript possesses several limitations that warrant consideration. Firstly, the training images were created through manual segmentation, which is a time-consuming process. The development of accurate automatic segmentation algorithms would be a valuable and progressive technical avenue for image analysis in future research. Secondly, the data were collected from a single institution, resulting in data homogeneity. To establish the clinical utility and generalizability of the model, further validation studies should be conducted using external datasets from different ethnic groups and regions. Finally, only traditional radiomics features were available in our study. Future research will explore comprehensive analysis by combining deep learning with traditional radiomics to improve the model and investigate the interpretability of the results.

Conclusion

In conclusion, this study found that the prevalence of the RMC in the 1555 mandibular sides was 27.2%, based on the analysis of CBCT images. A detection model for the RMC was developed by utilizing radiomic features extracted from panoramic radiographs and analyzing these features with four machine-learning algorithms. These algorithms demonstrated high performance in accurately differentiating the presence of the RMC and outperformed specialists.

Availability of Data and Materials

The datasets used and analyzed during the current study are available from the corresponding authors upon reasonable request.

Author Contributions

Conceptualization and design: DJZ, FW, YPQ, and QX. Data collection and curation: FW, LLH, YPQ, and DLZ. Methodology and Formal Analysis: DJZ and QX. Visualization: LY. Manuscript drafting was carried out by DJZ, FW, and LY, with key revisions being made by all authors. All authors have given final approval of the manuscript. All authors have agreed to take responsibility for all aspects of the work to ensure that questions related to the accuracy or integrity of any part of the work are appropriately investigated and resolved.

Ethics Approval and Consent to Participate

All procedures performed in this retrospective study were in accordance with the ethical standards of the national and institutional research committee and with the Helsinki Declaration of 1975, as revised in 2008. Approval was granted by the Medical Ethics Committee of the Hospital of Stomatology, Sun Yat-sen University (NO. KQEC-2023-14-01). Informed consent was deemed exempt by the Medical Ethics Committee of the Hospital of Stomatology, Sun Yat-sen University for this retrospective study.

Acknowledgment

Not applicable.

Funding

This research received no external funding.

Conflict of Interest

The authors declare no conflict of interest.

References

[1] von Arx T, Hänni A, Sendi P, Buser D, Bornstein MM. Radiographic study of the mandibular retromolar canal: an anatomic structure with clinical importance. Journal of Endodontics. 2011; 37: 1630–1635.

[2] Schejtman R, Devoto FC, Arias NH. The origin and distribution of the elements of the human mandibular retromolar canal. Archives of Oral Biology. 1967; 12: 1261–1268.

[3] Chávez-Lomeli ME, Mansilla Lory J, Pompa JA, Kjaer I. The human mandibular canal arises from three separate canals innervating different tooth groups. Journal of Dental Research. 1996; 75: 1540–1544.

[4] Kodera H, Hashimoto I. A case of mandibular retromolar canal: elements of nerves and arteries in this canal. Kaibogaku Zasshi. Journal of Anatomy. 1995; 70: 23–30. (In Japanese)

[5] Ossenberg NS. Retromolar foramen of the human mandible. American Journal of Physical Anthropology. 1987; 73: 119–128.

[6] Kikuta S, Iwanaga J, Nakamura K, Hino K, Nakamura M, Kusukawa J. The retromolar canals and foramina: radiographic observation and application to oral surgery. Surgical and Radiologic Anatomy. 2018; 40: 647–652.

[7] Bilecenoglu B, Tuncer N. Clinical and anatomical study of retromolar foramen and canal. Journal of Oral and Maxillofacial Surgery. 2006; 64: 1493–1497.

[8] Kim HJ, Kang H, Seo YS, Kim DK, Yu SK. Anatomic evaluation of the retromolar canal by histologic and radiologic analyses. Archives of Oral Biology. 2017; 81: 192–197.

[9] Sisman Y, Ercan-Sekerci A, Payveren-Arikan M, Sahman H. Diagnostic accuracy of cone-beam CT compared with panoramic images in predicting retromolar canal during extraction of impacted mandibular third molars. Medicina Oral, Patologia Oral Y Cirugia Bucal. 2015; 20: e74–e81.

[10] Auluck A, Pai KM, Mupparapu M. Multiple mandibular nerve canals: radiographic observations and clinical relevance. Report of 6 cases. Quintessence International. 2007; 38: 781–787.

[11] Lambin P, Leijenaar RTH, Deist TM, Peerlings J, de Jong EEC, van Timmeren J, *et al*. Radiomics: the bridge between medical imaging and personalized medicine. Nature Reviews. Clinical Oncology. 2017; 14: 749–762.

[12] Khanagar SB, Alfadley A, Alfouzan K, Awawdeh M, Alaqla A, Jamleh A. Developments and Performance of Artificial Intelligence Models Designed for Application in Endodontics: A Systematic Review. Diagnostics. 2023; 13: 414.

[13] Khanagar SB, Alkadi L, Alghilan MA, Kalagi S, Awawdeh M, Bijai LK, *et al*. Application and Performance of Artificial Intelligence (AI) in Oral Cancer Diagnosis and Prediction Using Histopathological Images: A Systematic Review. Biomedicines. 2023; 11: 1612.

[14] Alam MK, Abutayyem H, Kanwal B, A L Shayeb M. Future of Orthodontics-A Systematic Review and Meta-Analysis on the Emerging Trends in This Field. Journal of Clinical Medicine. 2023; 12: 532.

[15] Chaurasia A, Namachivayam A, Koca-Ünsal RB, Lee JH. Deep-learning performance in identifying and classifying dental implant systems from dental imaging: a systematic review and meta-analysis. Journal of Periodontal & Implant Science. 2024; 54: 3–12.

[16] Tabatabaian F, Vora SR, Mirabbasi S. Applications, functions, and accuracy of artificial intelligence in restorative dentistry: A literature review. Journal of Esthetic and Restorative Dentistry. 2023; 35: 842–859.

[17] Ozsari S, Güzel MS, Yılmaz D, Kamburoğlu K. A Comprehensive Review of Artificial Intelligence Based Algorithms Regarding Temporomandibular Joint Related Diseases. Diagnostics. 2023; 13: 2700.

[18] Karamifar K, Shirali D, Saghiri MA, Abbott PV. Retromolar canal infiltration as a supplement to the inferior alveolar nerve block injection: an uncontrolled clinical trial. Clinical Oral Investigations. 2021; 25: 5473–5478.

[19] Hanzelka T, Foltán R, Pavlíková G, Horká E, Sedý J. The role of intraoperative positioning of the inferior alveolar nerve on postoperative paresthesia after bilateral sagittal split osteotomy of the mandible: prospective clinical study. International Journal of Oral and Maxillofacial Surgery. 2011; 40: 901–906.

[20] Singh S. Aberrant buccal nerve encountered at third molar surgery. Oral Surgery, Oral Medicine, and Oral Pathology. 1981; 52: 142.

[21] Park MK, Jung W, Bae JH, Kwak HH. Anatomical and radiographic study of the mandibular retromolar canal. Journal of Dental Sciences. 2016; 11: 370–376.

[22] Iwanaga J, Watanabe K, Saga T, Tubbs RS, Tanaka K, Kikuta S, *et al*. A Novel Method for Observation of the Mandibular Foramen: Application to a Better Understanding of Dental Anatomy. Anatomical Record. 2017; 300: 1875–1880.

[23] Shan S, Zhong S, Li J, Wang T. Systematic review and meta-analysis of mandibular canal variations on cone beam computed tomography. Oral Radiology. 2022; 38: 445–451.

[24] Lizio G, Pelliccioni GA, Ghigi G, Fanelli A, Marchetti C. Radiographic assessment of the mandibular retromolar canal using cone-beam computed tomography. Acta Odontologica Scandinavica. 2013; 71: 650–655.

[25] Muinelo-Lorenzo J, Suárez-Quintanilla JA, Fernández-Alonso A, Marsillas-Rascado S, Suárez-Cunqueiro MM. Descriptive study of the bifid mandibular canals and retromolar foramina: cone beam CT vs panoramic radiography. Dento Maxillo Facial Radiology. 2014; 43: 20140090.

[26] Ogawa A, Fukuta Y, Nakasato H, Nakasato S. Evaluation by dental cone-beam computed tomography of the incidence and sites of branches of the inferior dental canal that supply mandibular third molars. The British Journal of Oral & Maxillofacial Surgery. 2016; 54: 1116–1120.

[27] Moreno Rabie C, Vranckx M, Rusque MI, Deambrosi C, Ockerman A, Politis C, *et al*. Anatomical relation of third molars and the retromolar canal. The British Journal of Oral & Maxillofacial Surgery. 2019; 57: 765–770.

[28] Nikkerdar N, Golshah A, Norouzi M, Falah-Kooshki S. Incidence and Anatomical Properties of Retromolar Canal in an Iranian Population: A Cone-Beam Computed Tomography Study. International Journal of Dentistry. 2020; 2020: 9178973.

[29] Palma LF, Buck AF, Kfouri FDÁ, Blachman IT, Lombardi LA, Cavalli MA. Evaluation of retromolar canals on cone beam computerized tomography scans and digital panoramic radiographs. Oral and Maxillofacial Surgery. 2017; 21: 307–312.

[30] Patil S, Matsuda Y, Nakajima K, Araki K, Okano T. Retromolar canals as observed on cone-beam computed tomography: their incidence, course, and characteristics. Oral Surgery, Oral Medicine, Oral Pathology and Oral Radiology. 2013; 115: 692–699.

[31] Capote TSDO, Gonçalves MDA, Campos JÁDB. Retromolar Canal Associated with Age, Side, Sex, Bifid Mandibular Canal, and Accessory Mental Foramen in Panoramic Radio-

graphs of Brazilians. Anatomy Research International. 2015; 2015: 434083.

[32] Fuentes R, Arias A, Farfán C, Astete N, Garay I, Navarro P, *et al*. Morphological variations of the mandibular canal in digital panoramic radiographs: a retrospective study in a Chilean population. Folia Morphologica. 2019; 78: 163–170.

[33] Hiraiwa T, Ariji Y, Fukuda M, Kise Y, Nakata K, Katsumata A, *et al*. A deep-learning artificial intelligence system for assessment of root morphology of the mandibular first molar on panoramic radiography. Dento Maxillo Facial Radiology. 2019; 48: 20180218.

[34] Zhang L, Xu F, Li Y, Zhang H, Xi Z, Xiang J, *et al*. A lightweight convolutional neural network model with receptive field block for C-shaped root canal detection in mandibular second molars. Scientific Reports. 2022; 12: 17373.

[35] Nakamoto T, Taguchi A, Kakimoto N. Osteoporosis screening support system from panoramic radiographs using deep learning by convolutional neural network. Dento Maxillo Facial Radiology. 2022; 51: 20220135.

[36] Zhou X, Yu G, Yin Q, Liu Y, Zhang Z, Sun J. Context Aware Convolutional Neural Network for Children Caries Diagnosis on Dental Panoramic Radiographs. Computational and Mathematical Methods in Medicine. 2022; 2022: 6029245.

[37] Lee YH, Won JH, Auh QS, Noh YK. Age group prediction with panoramic radiomorphometric parameters using machine learning algorithms. Scientific Reports. 2022; 12: 11703.

[38] Danks RP, Bano S, Orishko A, Tan HJ, Moreno Sancho F, D'Aiuto F, *et al*. Automating Periodontal bone loss measurement via dental landmark localisation. International Journal of Computer Assisted Radiology and Surgery. 2021; 16: 1189–1199.

[39] Greener JG, Kandathil SM, Moffat L, Jones DT. A guide to machine learning for biologists. Nature Reviews. Molecular Cell Biology. 2022; 23: 40–55.

[40] American Dental Association Council on Scientific Affairs. The use of cone-beam computed tomography in dentistry: an advisory statement from the American Dental Association Council on Scientific Affairs. Journal of the American Dental Association (1939). 2012; 143: 899–902.